Final Report for ACAS Summer School Group 1 Flight (B358 22/04/08, 08:32-10:59 UTC)

Thomas Hamburger[1], Karin Ardon[2], Daniel Perez[3], Benjamin Aouizerats[4], Helen Macintyre[5], Livio Belegante[6],.

1. DLR, Germany.
2. Tel Aviv University, Israel.
3. CEAMA, Universidad de Granada, Spain.
4. METEO-France, France.
5. School of Earth and Environment, University of Leeds, UK.
6. National Instute of R&D for Optoelectronics, Romania.

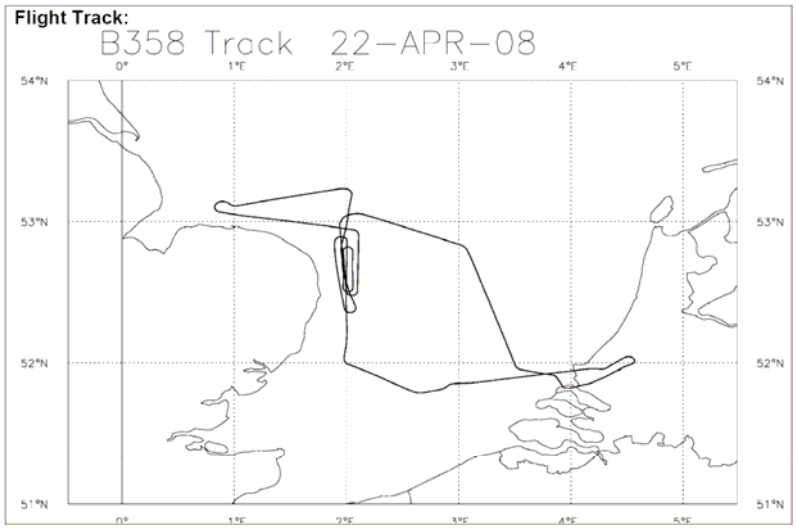

CONTENTS

Cover Images: The flight track for Flight B358, 22nd April 2008 (top). The view from 50ft above the North Sea (bottom).

1. INTRODUCTION AND AIMS OF THE FLIGHT.

Atmospheric aerosols play an important role in the Earth's climate system. They can modify the incoming solar and outgoing infrared radiation, as well as having various indirect effects via interactions with clouds (IPCC, 2007). These aerosols, consisting of sulfates, sea-salt, soot, organic carbon and mineral dust, are produced both naturally and by human activities (Satheesh, 2002). Whether aerosols warm or cool the planet depends on their chemical composition, and relative contribution of various chemical species, which constitute the aerosol (Satheesh, 2002).

For the North of Europe, sulfate is the dominant component above 1 km while particulate organic matter (POM) is dominant at the lower altitudes. For the South, dust is an important component above 1 km, mainly due to Saharan dust transport across the Mediterranean Sea, leading to larger values of the extinction coefficient in upper heights compared to the North (Matthias et al 2004)

A major unknown of the spatial aerosol distribution is the vertical distribution. Transport in the planetary boundary layer (PBL) and the free troposphere can be decoupled, resulting in different chemical composition, and thus aerosol optical properties in different layers (Guibert et al 2005).

The main aim of the flight is to investigate the atmospheric and aerosol properties of two different air masses, and look at the variation within them. In order to achieve this, runs will be planned in two different locations (which will depend heavily on the meteorology). We also wish to examine these properties within the boundary layer and above it (in the free troposphere). We therefore plan to make observations at different heights in our two locations (i.e. a 'stacked profile').

2. FLIGHT PREPARATION.

2.1 Forecast.

To achieve our objective of making a comparison between properties within the boundary layer and above it (in the free troposphere), we plan to make stacked profiles in two locations. The stacked profiles will consist of runs at two heights of 3000 and 9000 feet, as this will allow us to sample within the boundary layer and above it.

The first task when planning the flight is to examine the meteorological situation. The Met Office 24 hour forecast indicates an area of high pressure to the north and low pressure to the south, leading to a fairly steady easterly wind (Figure 1). This is expected to transport air to the region from two different source areas, from Scandinavia in the north and over the Black Sea in the south. It is expected that the air to the north and the air to the south to have different properties, as they have come from different source regions. Therefore a plan is made to make similar sets of measurements in the north and the south, in order to make a comparison.

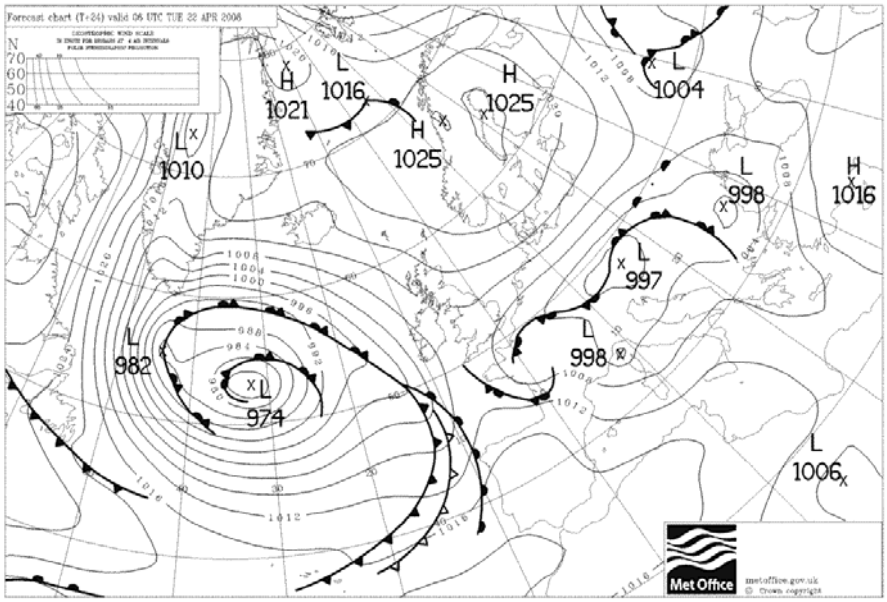

Figure 1: Synoptic forecast for 06UTC 22/04/08.

The forecast suggests that there is quite a low chance of cloud, due to the high pressure system to the north. For this reason it is decided that the CVI will be run in aerosol-mode rather than cloud-mode, in order to make the best use of the instrument in the prevalent conditions (see section 5 for a summary of instrumentation).

2.2 Dust layer.

2.2.1 Barcelona Supercomputing Centre:

A forecast from the Dust Regional Atmospheric Model (DREAM) from Barcelona Supercomputing Centre (http://www.bsc.es/projects/earthscience/DREAM/) indicated that there may be northward transport of dust to the region. Details of this model can be found in Nickovic et al., 2001. Here we give brief details. Basically, the concentration

equation simulates all major processes of the atmospheric dust cycle. During the model integration, calculation of the surface dust injection fluxes is made over the model points declared as deserts. Once injected into the air, dust aerosol is driven by the atmospheric model variables: by turbulent parameters in the early stage of the process when dust is lifted from the ground to the upper levels; by model winds in the later phases of the process when dust travels away from the sources; finally, by thermodynamic processes and rainfall of the atmospheric model and land cover features which provide wet and dry deposition of dust over the Earth surface. Therefore, special attention is made to properly parameterize dust production phase. Wind erosion of the soil in DREAM parameterization scheme is controlled mainly by the following factors: type of soil, type of vegetation cover, soil moisture content, and surface atmospheric turbulence. The major input data used to distinct the dust productive soils from the others are a global data set on land cover. In the current operational configuration of the model, four particle size classes (clay, small silt, large silt and sand) are estimated with particle size radii of 0.73, 6.1, 18 and 38 μm, respectively. For long-range transport, only the first two dust classes are relevant since their life time is larger than about 12 hours.

For the 22nd April 2008 we look into the model. In Figure 2, the predictions over our area of interest are marked with a red point. According to this model, we expected a thin dust layer in our interest area. However, we were not able to determine the altitude of the layer with only this information.

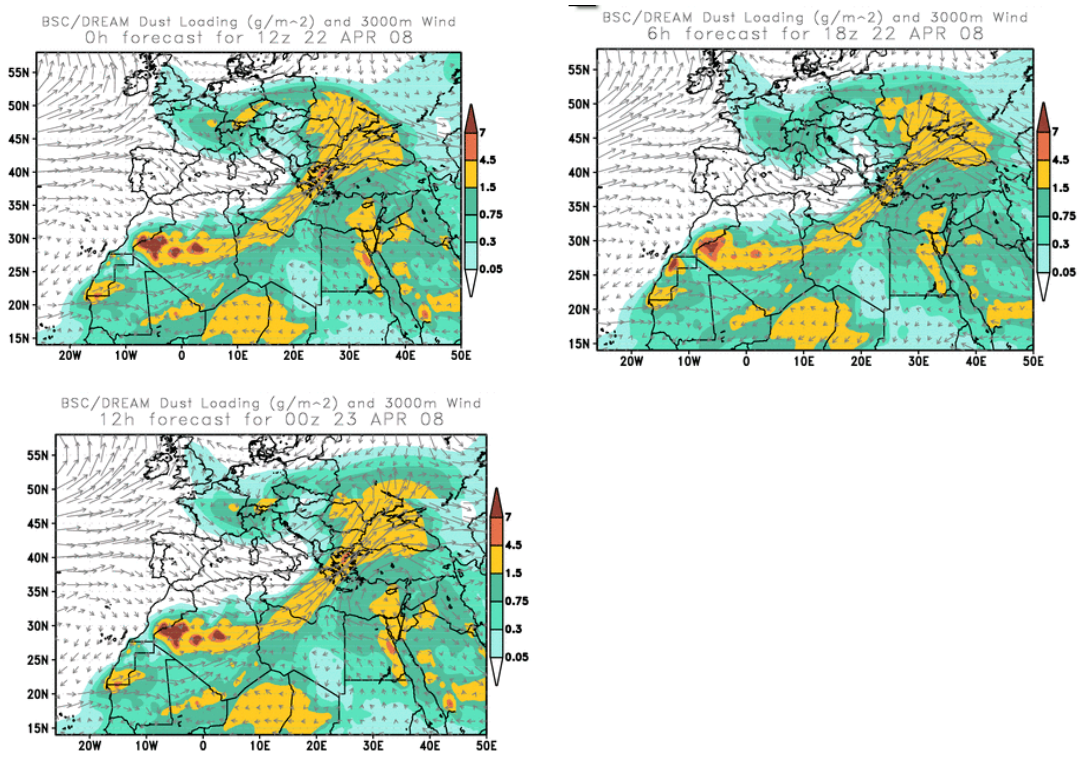

Figure 2: Dust loading in g/m^2 forecast over Europe predicted by DREAM for 22nd April 2008. a) 0 forecast. b) 6 h forecast. c) 12 h forecast

From Figure 2 a, b and c we can see that the dust load is between 0.05-0.5 g/m^2 and then it should be very weak (note that the dust load is given in g/m^2, and that it is the total

atmospheric column loading). Hence, we might have this dust layer in the surface or we might have the layer at certain height. In order to estimate the dust height we have to look to another model.

2.2.2 NAAPS Model

The DREAM model predicts a thin dust layer over our interest area but the height of the layer is still to be determined. In order to do this, we look at the NAAPS models (http://www.nrlmry.navy.mil/aerosol/ #currentaerosolmodeling). This model was developed by The Naval Research Laboratory (NRL) in Monterey, CA, for predicting the distribution of tropospheric aerosols. The model is a modified form of that developed by Christensen (1997). The model predicts the total optical depth at 500nm, and the surface concentration of sulphate, dust and smoke. Figure 3 shows us the surface dust concentration at 0, 6 and 12 hours in 22nd April 2008 (note that the dust load is given in $\mu g/m^3$, and that it is the total dust concentration in the atmospheric column). In this sense we must be careful when we compare Figure 2 with Figure 3.

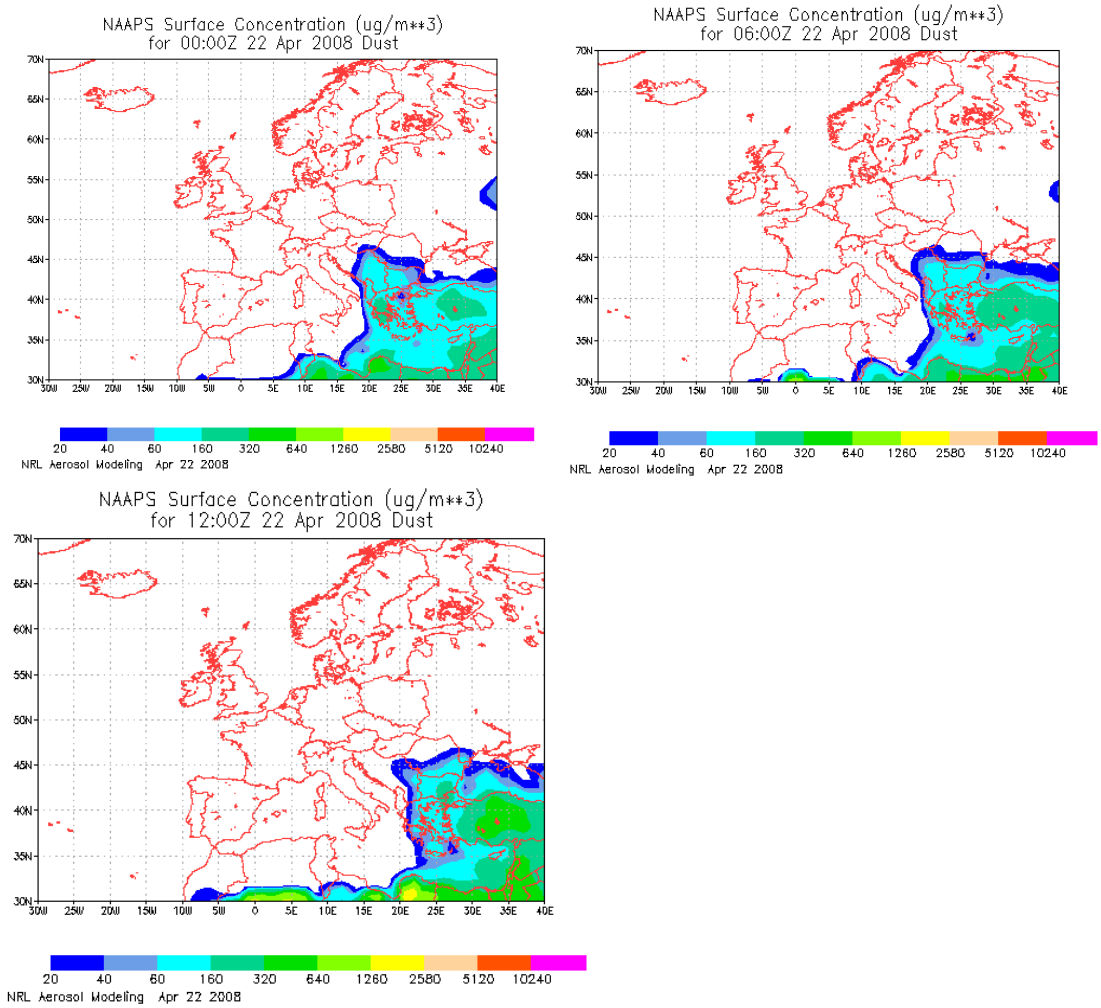

Figure 3: Dust surface concentration (g/m^3) from NAAPS model for 22nd April 2008.
a) 0 forecast. b) 6 h forecast. c) 12 h forecast.

From Figure 3, we can see that the dust concentration along the whole atmospheric column is negligible in our interest area. Hence, we can say that the dust layer should be at a certain height and must be quite weak.

2.2.3 LIDAR Data

In order to guarantee the existence of dust layer in our interest area we have a look to Lidar results from nearby stations to study the aerosol profile. A Lidar consists basically of a laser that emits light upwards. This light is backscattered by aerosol and molecules that are in the atmosphere, and with a correct treatment of this backscattered light, we are able to study aerosol atmospheric profile. More details about how Lidar systems work can be consulted in Weitkamp (2005) and Kovalev & Eichinger (2004).

So, thanks to the Institute for Tropospheric Research in Leipzig (Germany), we have the Lidar signal in Leipzig. Figure 4 shows the backscattered signal at 1064 nm from 10:00 to 17:20 at 1064 wavelength. From 0 to 2 km there is a strong backscattered signal. This is related to aerosol within the boundary layer in Leipzig. However, above the boundary layer we observe that there is a significant signal at about 4 km. This should be a thin dust load according to back trajectories analysis. Furthermore, this is a proof that there was a thin dust load over Northern Europe at this time. The strong backscattered signal at about 8-10 km is related to cirrus clouds.

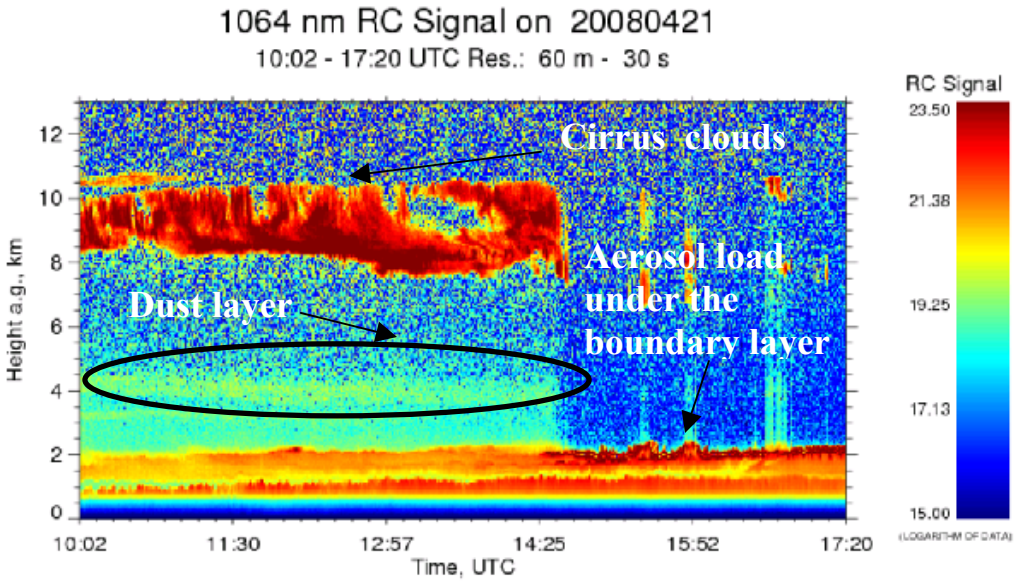

Figure 4. Lidar backscattered signal in Leipzig (Germany) the day before (21st April 2008) to our flight. A thin dust load is observed at about 4 km.

Furthermore, we follow the evolution of the dust layer in Leipzig. During the night, the dust layer was also very weak (graphics not shown here). For the next day, 22nd April, the dust went on, though it was weaker (Figure 5).

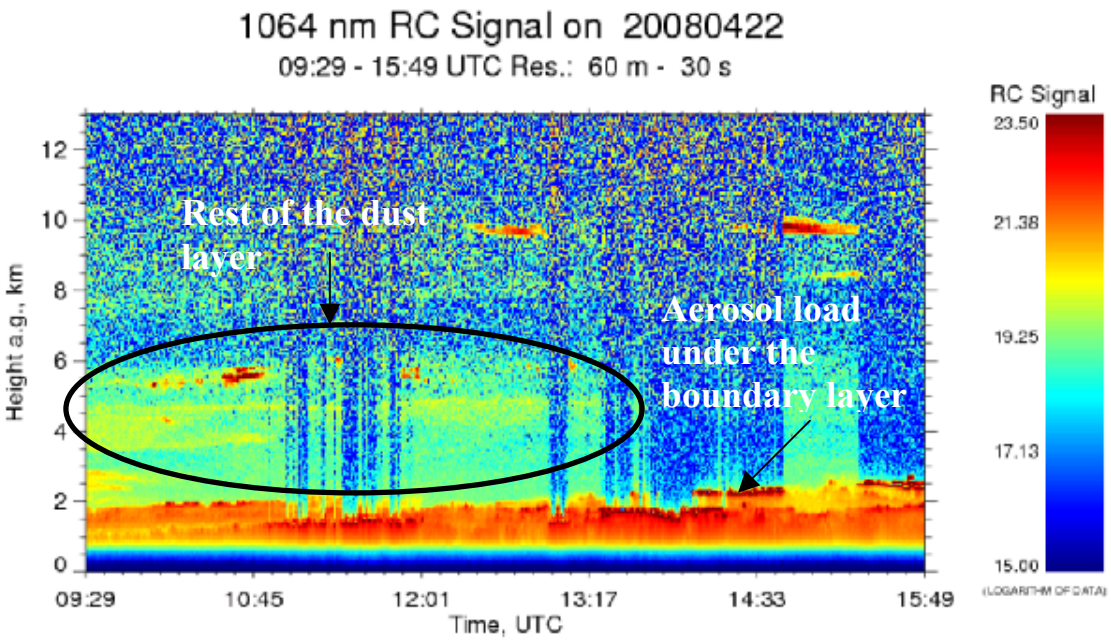

Figure 5.: Lidar signal at Leipzig (Germany) the day we carried out our flight (22nd April 2008). We can observe that there was still a residual at about 4km.

To sump up, according to the models and the Lidar data in a near station, we can say that there is a thin dust load in Northern Europe for 22nd April 2008. Due to this evidence for a dust layer in our study area, we decide to include a search for the dust layer in our flight plan.

3. FLIGHT PLAN – sortie brief.

Below is a copy of the sortie brief for the flight.

Flight B 358 **Date: Tues 22nd April 2008**

Mission Scientist: Dave Kindred

Briefing: 0530 UT (0730 local)
Take off: 0830 UT (1030 local)
Land: 1050 UT (1250 local)

Aim: To observe atmospheric and aerosol properties in the boundary layer and free troposphere in two different air masses.

Location: Southern North Sea

Weather conditions: Easterly winds, clear sky, chance of low cloud.

Key instruments: Aerosol properties and trace gas instruments.

Sortie Detail:

#	Time (Z)	Manoeuvre	Duration
1.		Leave Rotterdam. Travel west at 1000 ft. Ship tracks near Felixstowe.	**35 min**
2.		Stacked-vertical profile from 1000ft – FL90. a. Run at 3,000ft (6 min) (A => B) b. Run at FL90 (5 min) (A => B)	**28 min**
3.		Profile to locate dust layer (estimated at FL120) climbing at 1000fpm. Run at 1000ft above the dust layer (4 min) and a run within it (5 min). All this is done travelling north.	**14 min**
4.		Stacked-vertical profile from FL120 – 3,000ft at location further north than the first one. a. Run at FL90 (5 min) (C => D) b. Run at 3,000ft (6 min) (D => C)	**23 min**
5.		Return transit to Rotterdam.	**40 min**
6.		**Total time: 2hrs 20 min**	

4. IN-FLIGHT MODIFICATION.

The flight was quite successful, and the majority of the objectives were achieved. However, as with all campaigns of this nature, there had to be some in-flight modification of the flight plan. A review of these is given below.

4.1 Location of the ship plumes.

Since the location of the ship plumes could not be predicted, observation of these had to be performed on an *ad hoc* basis. Ships were located visually and the pilots were able to manoeuvre into a position in order to sample them. Ship plumes were crossed (perpendicular to ship motion), but due to aircraft speed this would only give a very small sampling period. So when feasible we manoeuvred to a position where we could fly following one of the plumes, thus increasing our chances of collecting data for the plumes. This was completed successfully on the flight, and so sampling of these was achieved.

4.2 Locating the dust layer.

The most uncertain aspect of the flight was searching for the dust layer at FL120. Prior to the flight we had to come up with a contingency for if we did not manage to locate the dust layer. However, we found some weak evidence of the layer, so we looked for it for a short time. Observations were made in and around where we thought the layer was. The forecast provided us with an indication of the height we could expect to find the dust, but we did not know for sure the height until we saw the observations during the flight. We also did not know the thickness, so a close watch on the instrument was kept during the flight.

4.3 North and south stacked profiles.

An important flight corridor is situated over the North Sea coming across the north of East Anglia and then turning towards Rotterdam. When we approached this it was necessary to check with local ATC (Air Traffic Control) to ensure it was possible for us to fly further north to take the second set of runs. However, it was not possible fro us to do this during the flight. Instead we decided to take the profiles and make the runs where it was possible to do this with as little alteration to the original plan as possible.

4.4 Time constraints.

The time available for the flight was relatively short (2h 20min total flight time). In order to make the most use of the time we had, a minute-by-minute plan was formulated. In our flight brief, the most uncertain aspect of the time constraint was the part for locating the dust, as we did not know if it would be seen or not. The time we needed to spend on this may have been underestimated, as we were behind schedule at the end of the dust runs. We had to decide how best to use our remaining time. Since our main objective was to make observations within the boundary layer and above it, it

was decided to make a run at 9000ft (to match the runs at the beginning), and then quickly descend to 3000ft to make the corresponding run here. This meant that we could not take profile observations on the descent, but it was decided that this could be sacrificed in place of making runs at 9000ft and 3000ft, as these are more important to the objectives.

5. INSTRUMENTATION.

A summary of some of the main instruments used on the fight follows.

- Counter flow Virtual Impactor:

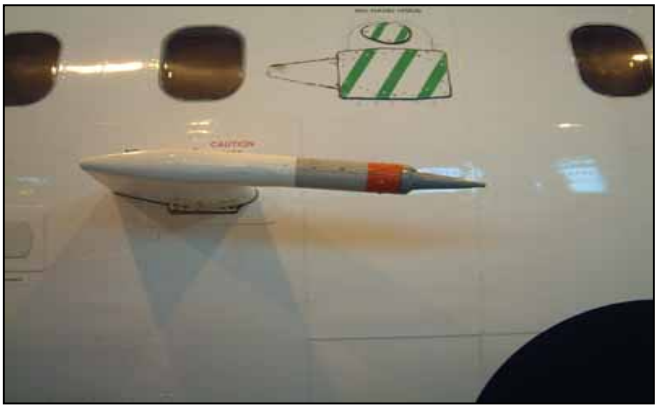

Designed by the University of Stockholm, the CVI is a device aiming at counting cloud droplets by removing them from the airflow and evaporate them, leaving the residual particles and the water vapour. The range of the CVI is from 10 nm. The principle of the CVI is based on the virtual inertial impaction of accelerated cloud elements. The acceleration results from the air speed of the aircraft or from a wind tunnel in front of the CVI. The inlet tubing is equipped with a porous tube through which the so-called supply flow is fed in. The main part of this flow is sucked as so-called sample flow by the instruments. A small flow of excess air streams as so-called counter flow out of the inlet tip against the accelerated cloud air. That way a stagnation plane is created in the tube. Hydrometeors with sufficient inertia to reach this plane are sampled via the sample flow, while interstitial particles are stopped before and removed from the inlet by the counterflow.

- Nephelometer:

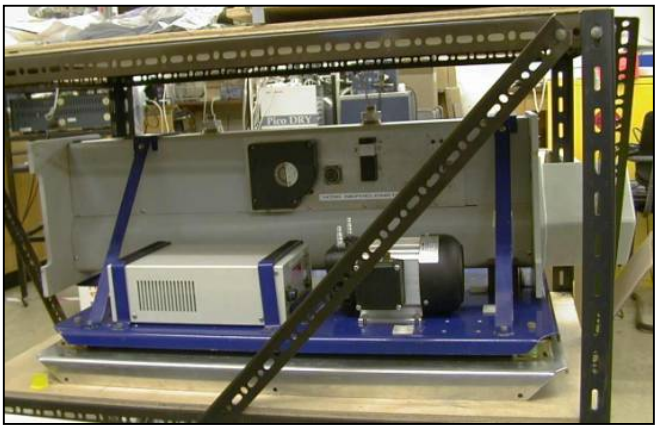

The nephalometer installed in the BAe measures the total scattering coefficients from 7° to 170° and the hemispheric scattering coefficients from 90° to 170°.
With the measurements at three different wavelengths (450, 550 and 700nm), the nephelometer provides atmospheric visibility, radiative forcing or the extinction budget pertaining to aerosol particles.

- Broad Band Radiometers:

The BRB contains the following core instruments:

- Clear Dome Pyranometer : 0.3 - 3µm hemispheric irradiance
- Red Dome Pyranometer : 0.7 - 3µm hemispheric irradiance
- Pyrgeometer: 4 - 50µ hemispheric irradiance.

These instruments provide every second an integrated value for the upwelling and downwelling irradiances.

- Core Chemistry Rack:

This rack contains the following instruments:

- TECO 49 UV photometric instrument to measure O_3.
- TECO 42 chemiluminescence to measure NO, NO_2 and NO_x.
- TECO 43C trace gas analyser to measure SO_2.
- Aero-Laser Gmbh AL5002 Fast Carbon Monoxide (CO) Monitor.

- Four Video cameras were also placed in the front, in the back, on the top and above the plane. Two from these four cameras were recording during the flight.

- Wing Pylons:

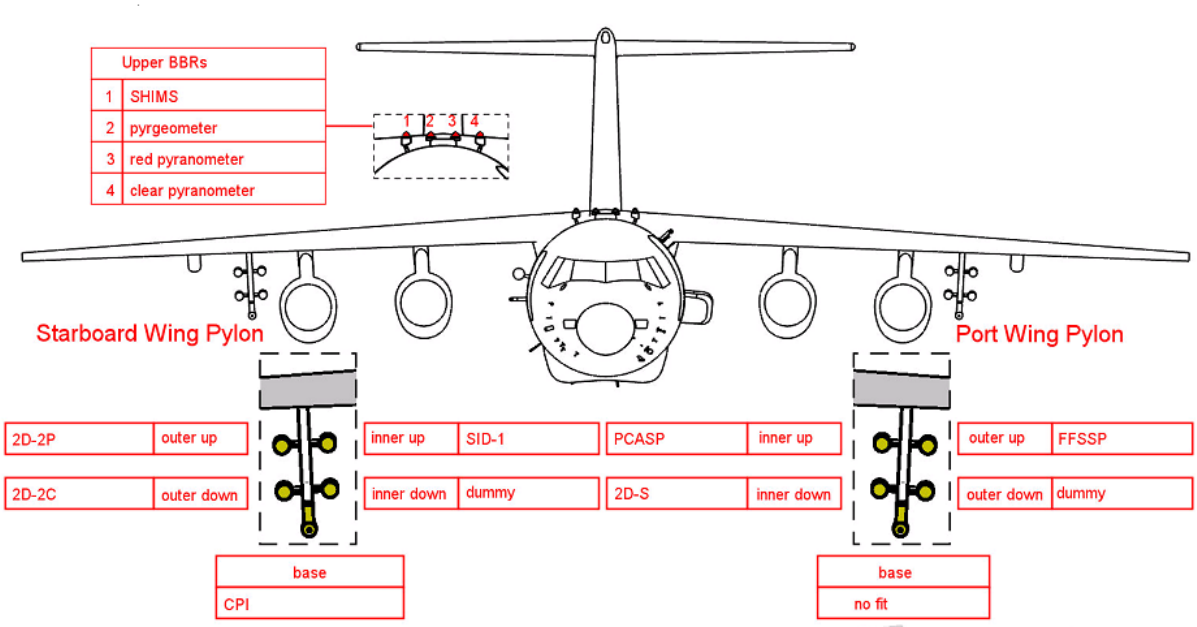

→ 2D-2P: The 2D-P aims at measuring the size spectrum of ice crystals and water droplets within a range from 200 µm to 6400 µm. Every 5 seconds, the device provides the particle number concentration, the condensed water content, the mean volume radius, the precipitation rate and the size spectrum.

→ 2D-2C: Similar to the 2D-P, The 2D-C measures the particle number concentration, the condensed water content, the mean volume radius, the precipitation rate and the size spectrum but within a range from 50 μm to 800 μm.

→ SID-1: The small ice detector was developed by the University of Hertfordshire. It measures the spherical equivalent size sprectum, within a range from 1 μm to 50 μm.

→ PCASP: This device measures the aerosol size spectrum within a range from 0.1 μm to 3 μm and provides an integrated value of aerosol particle concentration, mean volume radius and size spectrum every second.

→ Fast FSSP: The fast FSSP provides every second an integrated value of droplet number concentration, liquid water content, mean volume radius, effective radius and droplet size spectrum within a range from 1 μm to 50 μm.

- Condensation Particle Counter:

The Model 3025A uses a vapour sheath technique to improve the instrument's lower particle size sensitivity. This means that the counter is capable of measuring the number concentration of submicrometer airborne particles that are larger than 3 nanometers in diameter. Submicrometer particles are drawn into the counter and enlarged by condensation of a supersaturated vapour into droplets that measure several micrometers in diameter. The droplets pass through a lighted viewing volume where they scatter light. The scattered-light pulses are collected by a photodetector and converted into electrical pulses. The electrical pulses are then counted and their rate (calculated) is a measure of particle concentration

6. INTERPRETATION OF OBSERVATIONS.

6.1 Analysis of the meteorological situation.

In this part of the scientific report the meteorological situation during the FAAM flight b358 on Tuesday 22-April-2008 will be examined by using ECMWF analysis data and airborne measured meteorological data. Afterwards we will have a closer look on the atmospheric transport situation using the lagrangian trajectory tool LAGRANTO.

6.1.1 Synoptic overview.

The data used for the meteorological analysis is provided by the European Centre for Medium-Range Weather Forecasts ECMWF. The data used is taken from the operational archive. The model has the spectral resolution T799L91 i.e. a horizontal grid of 0.225°x0.225° and 91 vertical levels.

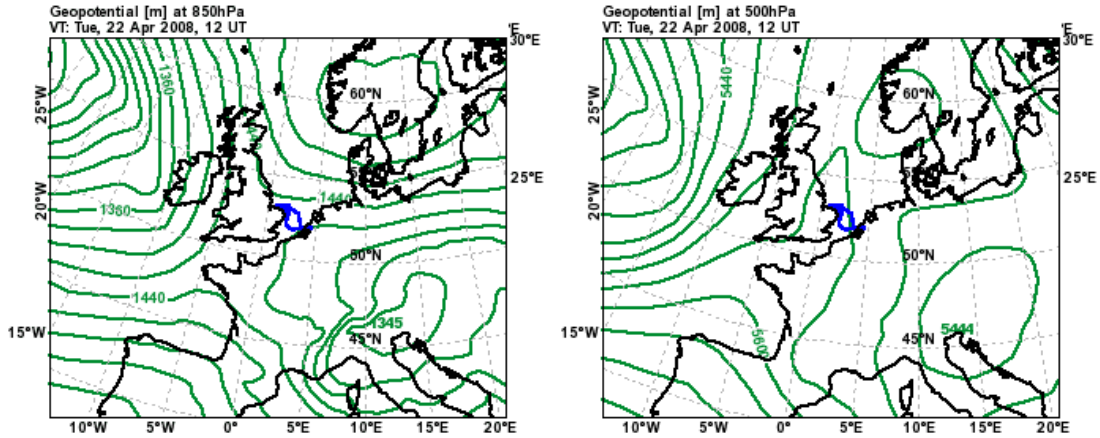

Figure 6: Geopotential height at 850 hPa and 500 hPa from the operational archive from the ECMWF at 22-April-2008, 12:00 UT.

Figure 6 shows the geopotential height at 850 hPa and 500 hPa, 22-April-2008, 12:00 UT. The flight track is also shown in blue. A high pressure system with its centre over southern Norway and Sweden leads with a low pressure system over northern Italy and Austria to a easterly flow in lower levels at the southern coastlines of the North Sea and Baltic Sea. Although the wind velocity increases with latitude in the region of the flight between the Dutch and English coast, only weak easterly winds with a light northward component dominate the flow over the Northern Sea at 850 hPa. At 500 hPa the wind field on the eastern part of the flight track turns to northerly winds while it remains easterly over northern Germany. At the western part of the flight track nearly no wind occurs at 500 hPa due to horizontal wind shear to the west induced by an approaching low pressure system over the Atlantic.

Figure 7 shows the relative humidity at 850 hPa and 500 hPa. While the moisture field in Southern and in Western Europe is dominated by the frontal systems of the two low pressure systems over the Atlantic and northern Italy, relatively dry air masses can be found over the North Sea. The moisture increases at 850 hPa over the Netherlands and Belgium because of shallow convection over land at 12:00 UT. On the MSG (Meteosat Second Generation) image in Figure 8, one can see that the increasing moisture at lower levels over the Netherlands could not lead to low level clouds during the time of the

flight. Also at 12:00 UT the MSG imagery does not show low level respectively boundary layer clouds (not shown here). Only some thin Cirrus and persistent contrails occurred above the flight area during the flight caused by slow ascending air masses in the upper troposphere due to the approaching low pressure system over the Atlantic.

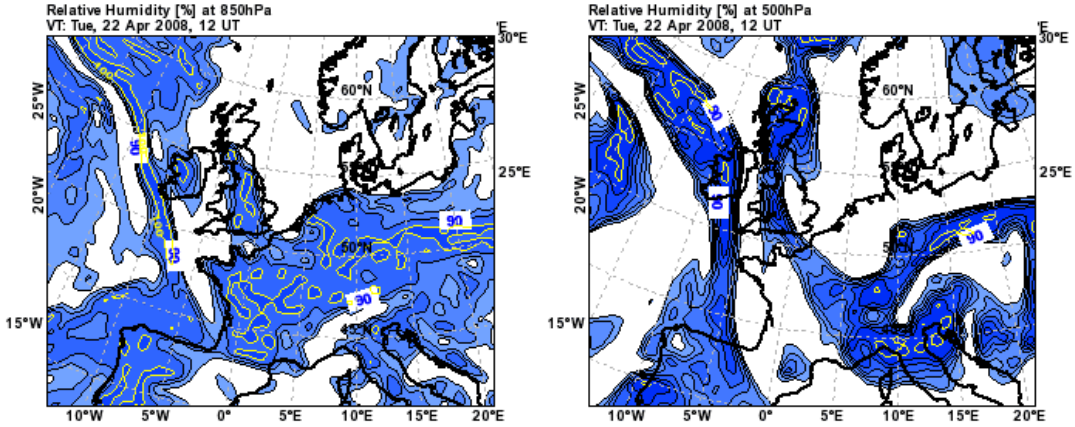

Figure. 7: Relative humidity at 850 hPa and 500 hPa from the operational archive from the ECMWF at 22-April-2008, 12:00 UT. The minimum values for the contours are 70% at 850 hPa and 40% at 500 hPa. Yellow lines indicate relative humidity of 100%.

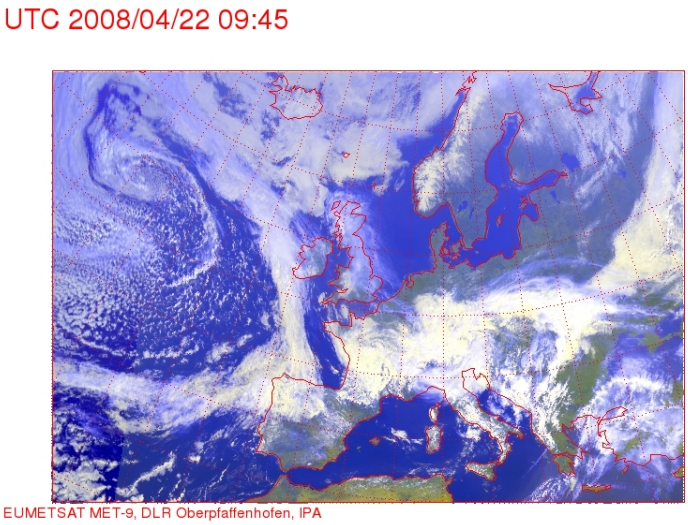

Fig. 8: Meteosat Second Generation (MSG) false colour composite image at 22-April-2008, 09:45 UT.

6.1.2 Boundary Layer.

Because of the high pressure system over southern Scandinavia which was described above, a very stable layered air mass could develop throughout the troposphere above the North Sea and the Netherlands. Figure 9 shows the vertical distribution of temperature and dew point temperature measured during the flight and during a sounding at De Bilt at 12:00 UT. Above a quite moist boundary layer, an inversion layer between 1350 m and 1750 m developed and separates the boundary layer from the dry free troposphere. While the boundary layer height above the North Sea (at the time of the flight) was located at about 1350 m, the boundary layer height at De Bilt is a little bit higher at about 1650 m. This can be caused by stronger convection above land or by the later time of the measurements at 12:00 UT, and thus a higher boundary layer top.

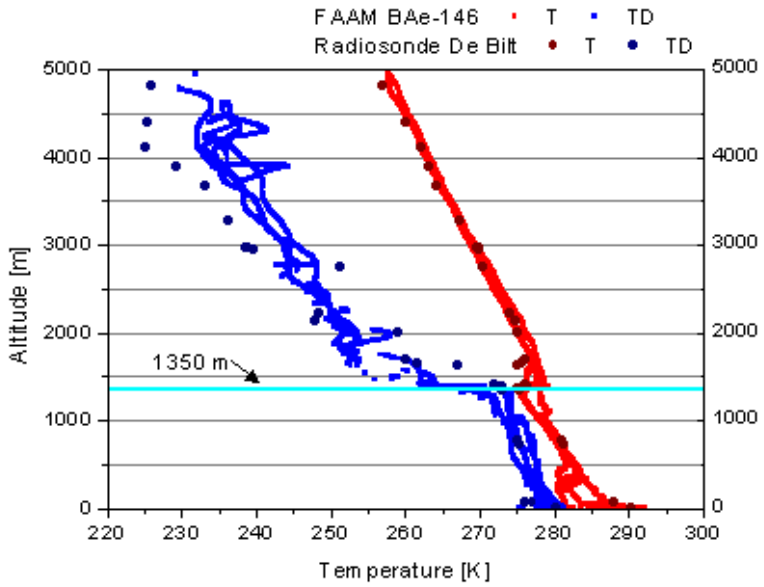

Figure 9: Plot of temperature (red) and dew point temperature (blue) versus altitude. The data was derived from measurements during the flight at 22-April-2008 and from radiosonde measurements (dark blue and dark red dots) at De Bilt at 12:00 UT.

The transport situation inside the boundary layer is shown in Figure 10 from the LAGRANTO trajectory model. Information about the model can be found in Wernli and Davies (1997) and Stohl et al (2001). The calculation time step which was used for the trajectory calculation is 30 minutes and the time increment of the ECMWF input data is 3 hours. The trajectories show a westward transport of the air masses

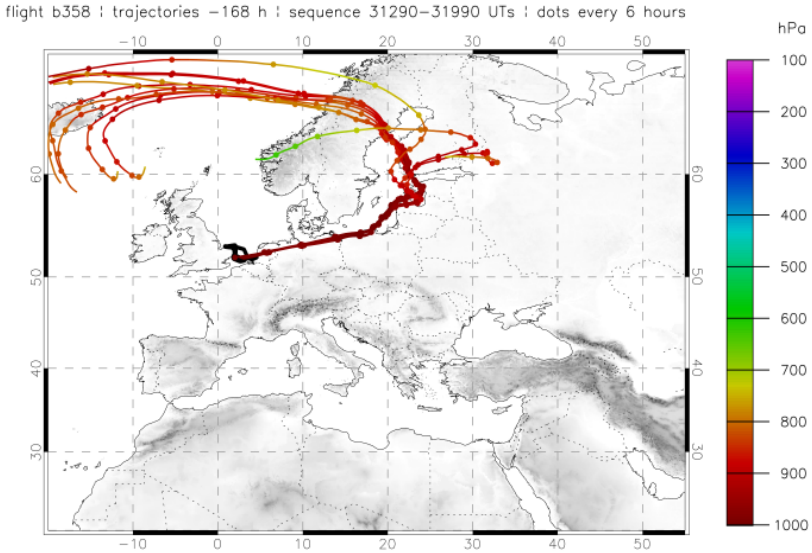

Figure. 10: LAGRANTO backward trajectories -168 hours taken from the flight sequence between 08:41 UT – 08:53 UT at 230 m.

along the southern coast line of the Baltic Sea, northern Germany and the Netherlands towards the North Sea. For at least 48 hours the transport takes place at very low levels without any mixing of tropospheric air into the boundary layer.

In addition, with the inversion described above and the low wind speeds in the southern parts of the Northern Sea, the pollution and emissions of northern Germany and the Netherlands which have been transported by easterlies towards the Northern Sea, could accumulate in the boundary layer. Also the lack of cloud formation and precipitation led to a high load of pollution inside the boundary layer, which could be measured during the flight.

6.2 Boundary layer – free troposphere comparison.

This is a comparison of various measured properties within the boundary layer and above it (i.e. in the free troposphere). The measurements in the boundary layer were at 3000ft, and the free troposphere measurements were at 9000ft. Figure 11 shows the flight trajectory.

For the A-B measurement (refer to Figure 11), the average altitude of the first measurement in the boundary layer was 3135.03 feet with a total sampling time of 00:06:09 (hh:mm:sec). The second measurement's average altitude above the boundary layer was 9042.26 feet for a total time of 00:05:34 (hh:mm:sec).

For the C-D measurement, the average altitude of the first measurement above the boundary layer was 9068.69 feet with a total sampling time of 00:04:02 (hh:mm:sec). The second measurement's average altitude above the boundary layer was 3154.06 feet for a total time of 00:04:11 (hh:mm:sec).

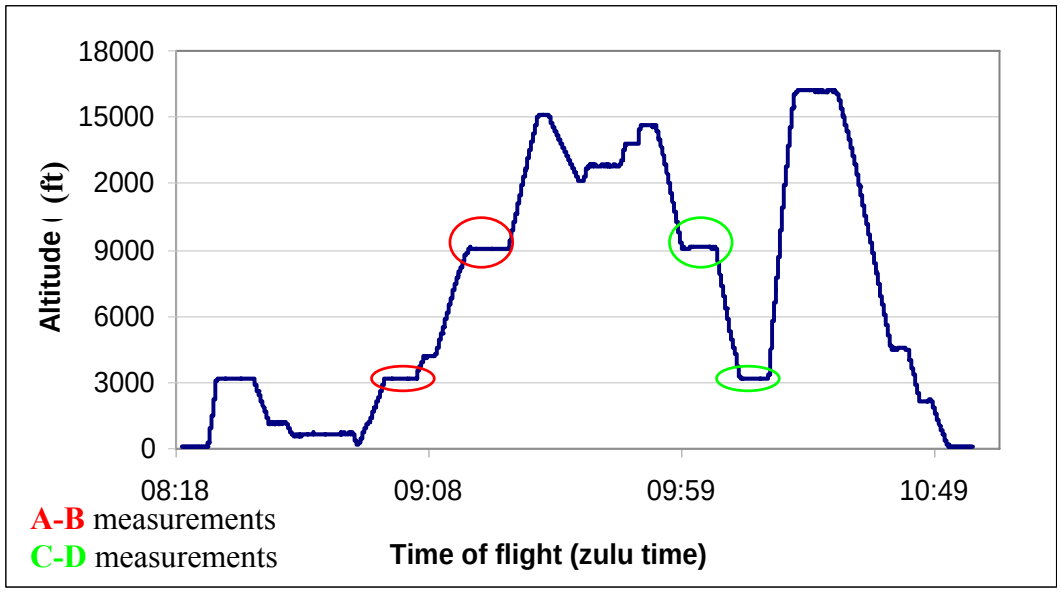

Figure 11: comparison between the two trajectories regards to the time of flight and the altitude. Red: the first measurement from A-B, green: the second measurement from C-D.

Difference between measurement in and above the boundary layer (BL) found in different component such as dew point values, aerosol concentration and the chemical concentration.

	Altitude of measurements	Start measurement Latitude	Start measurement Longitude	End measurement Latitude	End measurement Longitude
A-B	3000	52.386	1.999	52.754	2.003
	9000	52.415	2.073	52.783	1.954

C-D	3000	52.532	1.970	52.776	1.967
	9000	52.512	1.998	52.781	1.971

Table 1: Latitude and Longitude of the trajectories at different height

6.2.1 Dew point

The dew point value which indicates the amount of moisture in the air is higher in the boundary layer than the values measured above the boundary layer (Figure 12). We can claim that the air in the boundary layer is more humid than the air measured above the boundary layer, which is much dryer. A similar result was found by Gunter (2007).

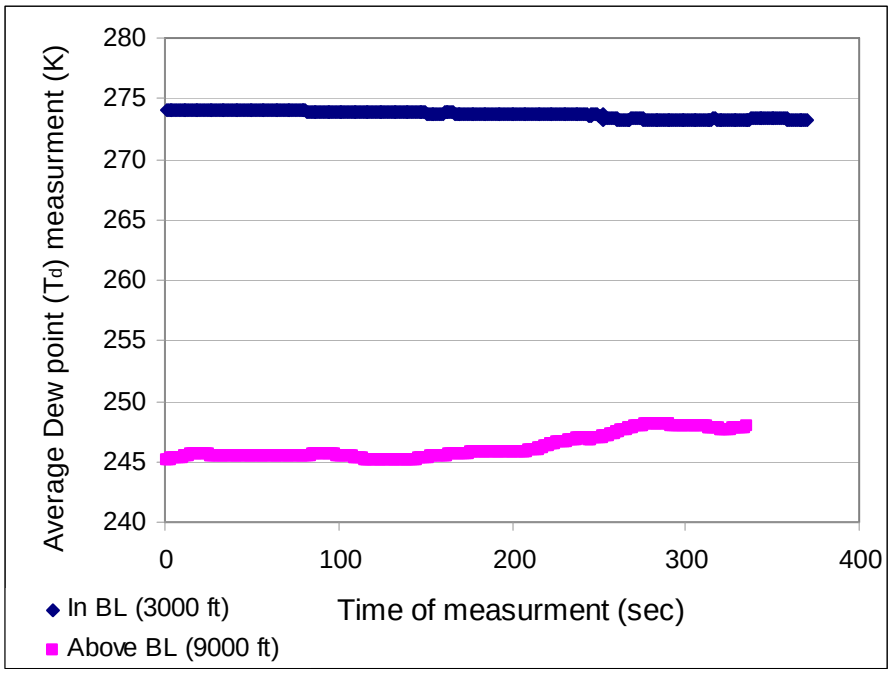

Figure 12: comparison between dew point value in and above the boundary.

6.2.2 Aerosol concentration

The amount of aerosol measured at the two altitudes was different in most cases by an order of magnitude. According to Baron and Willeke (2001) vertical distribution shows an exponential decrease with latitude.

In our experiment there is a big difference between the aerosol measurement taken in and above the boundary layer. From the literature, it is known that at a lower altitude the aerosol concentration is higher than at a higher altitude (Ferrare et al., 2005; Ferrare et al., 2006; Parameswaran et al., 2001; Guibert et al., 2005).

The observation from the Condensation Particle Counter (CPC) in the boundary layer was 3736.9 (counts per cc), more than 5 times that measured above the boundary layer (684.5 counts per cc). The higher aerosol concentrations within the boundary layer is because this layer has, by definition, contact to the ground and the majority of aerosol sources are at ground level (Matthias and Bösenberg, 2002).

The average droplet concentration from PCASP (channels 2-14 only) is higher for measurement taken in the boundary layer (964.03±107) in compared to those taken above it (26.21± 17) (Figure 13). The mass content from PCASP (channels 2-14 only)

was higher in the boundary layer (0.00715 ± 0.003 milligram m^{-3}) by an order of magnitude in comparison to the mass content measured above the boundary layer (0.00042 ±0.002 milligram m^{-3}).

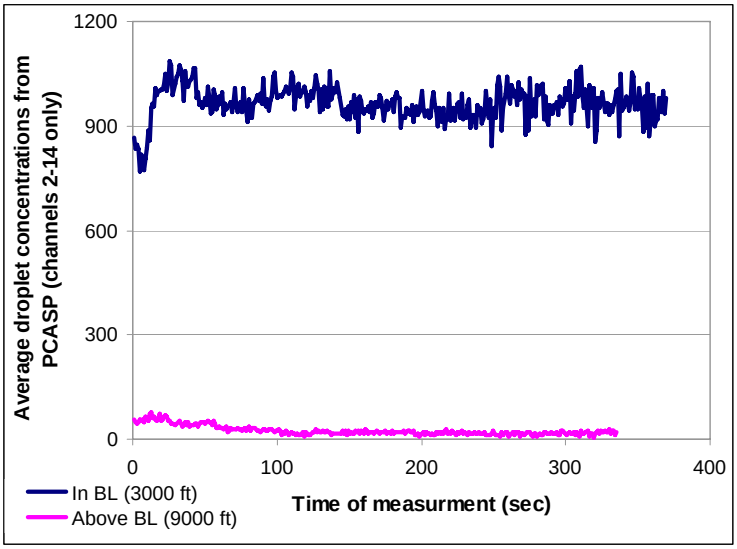

Figure 13: comparison between average droplet concentrations measured by PCASP (2-14 channels) in and above the boundary layer.

Particle diameter analyses using the PCASP reveal little difference for particles smaller than 0.17µm and greater than 0.95µm. However, there is a large difference in size distribution between the two measurements taken in and above the boundary layer is in the median size (0.17µm<X<0.95µm) (see Figure 14).

The small difference in size distribution for particle diameter, ranging between 0.17µm>X>0.95µm can come from the difference between each measurement. As can be seen in Figure 15, there is a difference in the PCASP measurement between the first and second measurements.

The source for the aerosol we measured during the flight came from the east, from Europe, as can be seen by the backward trajectory analysis (Figure 16). The backward trajectory analysis employed to examine the transport process of the air mass. The analysis in this paper is based on the HYSPLIT4 (HYbrid Single-Particle Lagrangian Integrated Trajectory) taken from NOAA ARL (2008).

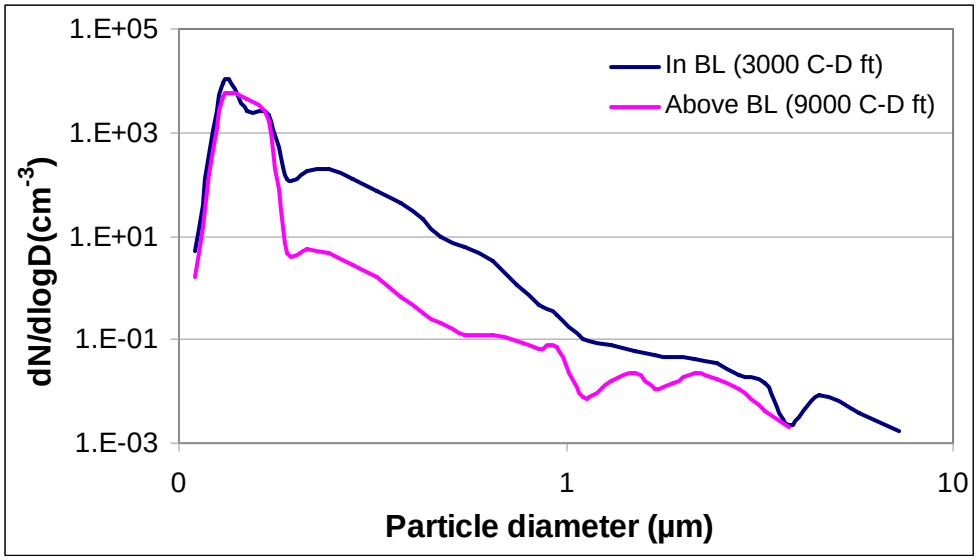

Figure 14: comparison between average size distributions measured by PCASP in and above the boundary layer.

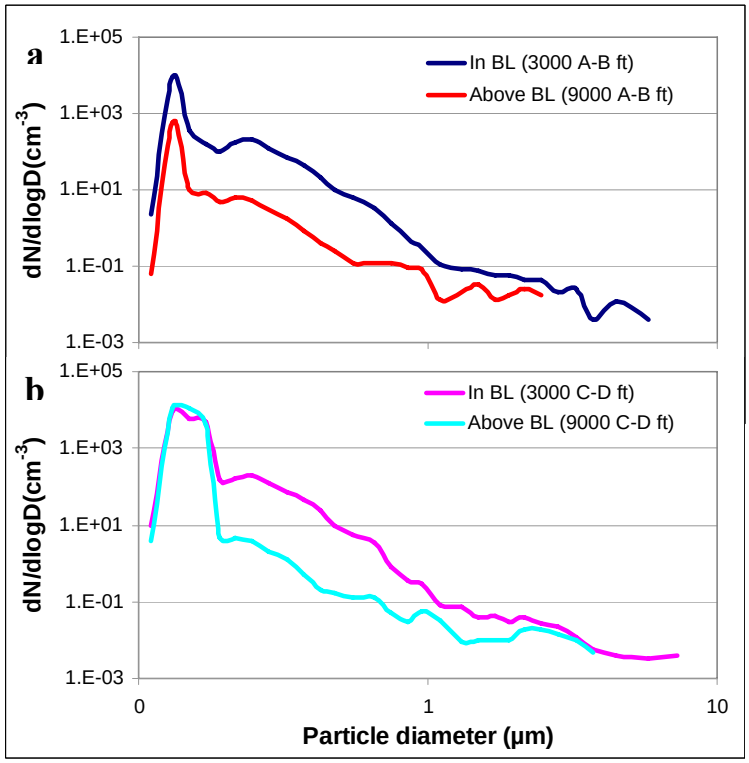

Figure 15: comparison between average size distributions measured by PCASP in and above the boundary layer for the two trajectories: a- for A-B measurement, b- for C-D measurement.

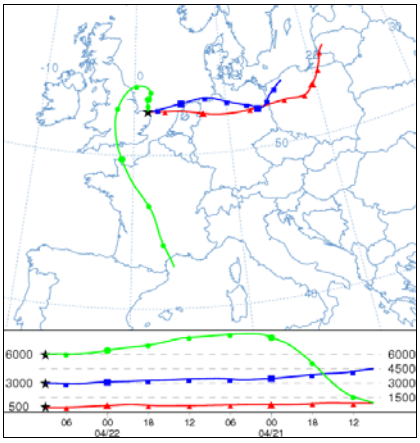

Figure 16: backward trajectory analysis for the transport of the air mass during the time of the flight for three different heights (500, 1500 and 3000m).

Considering the fact that the measurements were taken in a marine area we can say that among various types of tropospheric aerosols, maritime aerosols are expected to exhibit particularly large variability. Occasionally, particles transported from urban, industrial, and/or desert areas are mixed with indigenous (maritime) aerosols. These findings infer that parts of the marine aerosols are greatly influenced by nearby aerosol sources (on land surfaces), emphasizing the importance of the air mass transportation (Ooki et al., 2002).

6.2.3 Chemical concentration

Significant differences in NO_x (NO_x = NO + NO_2) concentrations were found in and above the boundary layer. Aerosol nitrate is regionally important but its global impact is still uncertain. Oxides of nitrogen can indirectly affect the Earth's radiative balance as they provide a source of ozone via photolysis of NO_2 and reaction with oxygen (IPCC 2001). Higher levels of nitrous oxides were found in the boundary rather than above the boundary layer (Figure 17). Higher values of NO_2 were measured compared to NO. This could be due to the fact that most tropospheric NO_x is emitted as NO, which photo-chemically equilibrates with NO_2 within a few minutes (IPCC 2001).
No significant differences were found for the mole fraction of ozone measurement.

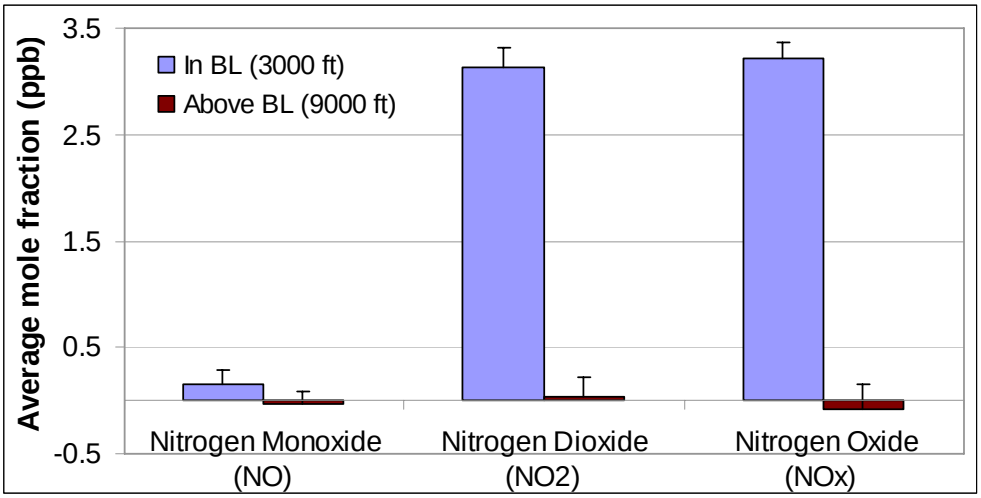

Figure 17: Comparison between chemical concentration in and above the boundary layer for nitrogen oxide (NO), nitrogen dioxide (NO_2) and nitrous oxides (NO_x).

6.3 Nephelometer Data Analysis

In this section we are going to analyze the data from the nephelometer TSI-3563. This instrument is able to measure both total scattering and backscattering coefficient at three different wavelengths, 450, 550 and 700 nm. To simplify our calculation, we work only with the total scattering coefficient τ_{scat}. This coefficient is the total amount of light scattered per longitude unit by volume of particles.

Furthermore, we use the Amstrong law for particle attenuation. This law tells us that the attenuation particles depends on the wavelength and can be written as follows:

$$\tau_{ext} = \beta \cdot \left(\frac{\lambda}{\lambda_0} \right)^{-\alpha}$$

Where λ is the wavelength, λ_0 is the wavelength at 1000 μm, β is the extinction at 1000 μm and α is parameter that tells us if big/small particles predominate. In this work, to facilitate the analysis, we suppose $\tau_{ext} \approx \tau_{scat.}$ In the next table we show the typical α parameter range for different aerosol types. This range has been retrieved from different AERONET (http://aeronet.gsfc.nasa.gov/) network of ground-based radiometer (Dubovik et al., 2001).

Aerosol Type	**α Range**
Urban-Industrial and mixed	$1.2 \leq \alpha \leq 2.5$
Biomass Burning	$1.2 \leq \alpha \leq 2.1$
Desert dust and oceanic	$0 \leq \alpha \leq 1.6$ and $0.1 \leq \alpha \leq 0.9$

Table 2.: Range of α parameter for different aerosol particles. The data have been retrieved from different AERONET sites (Dubovik et al., 2001).

In Figure 18 we show the total scattering coefficient measured by the nephelometer. The total scattering coefficient has been multiplied by 10^6 and it is expressed in Mm^{-1}. Blue represents the 400 nm channel, green the 500 nm and red the 700 nm. Once we have measurements at this wavelengths, we can calculate alpha parameter by fitting $\log(\tau_{ext})$ versus $\log(\lambda)$.

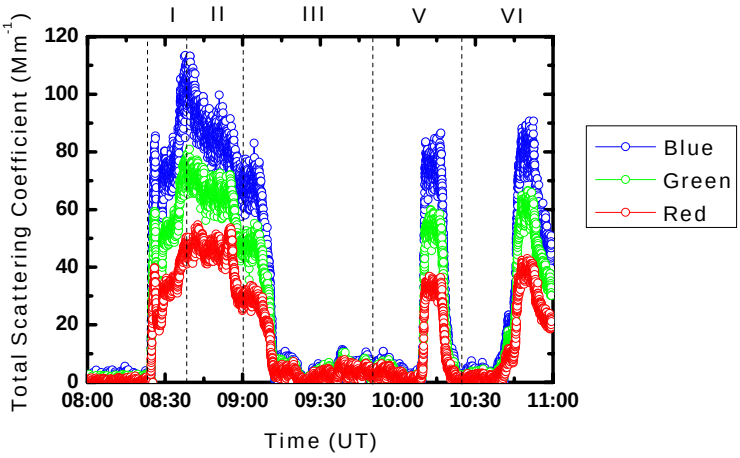

Figure 18: Total scattering coefficient measured by the nephelometer TSI-3563 for the flight B358 (22nd April 2008). Roman numerals along the top refer to different zones. See text for details.

According to our flight briefing, we have divided Figure 18 into different parts to show the different atmosphere's area we measured.

· ZONE I: Take off Airport-Sea

These measurements were made while the plane took off. This was the time in which the plane took off from the airport, flew over Rotterdam industrial area and later arrived to the Netherlands coast.

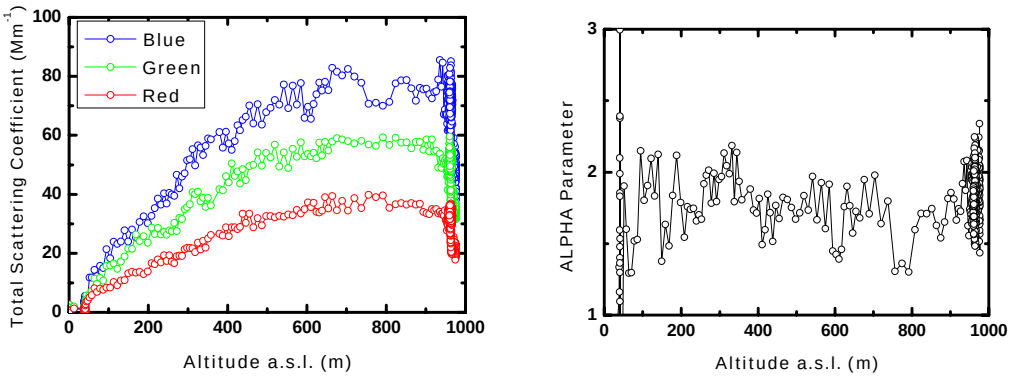

Figure 19: Total scattering coefficient and alpha parameter variation with altitude. The data were retrieved while the plane was taking off.

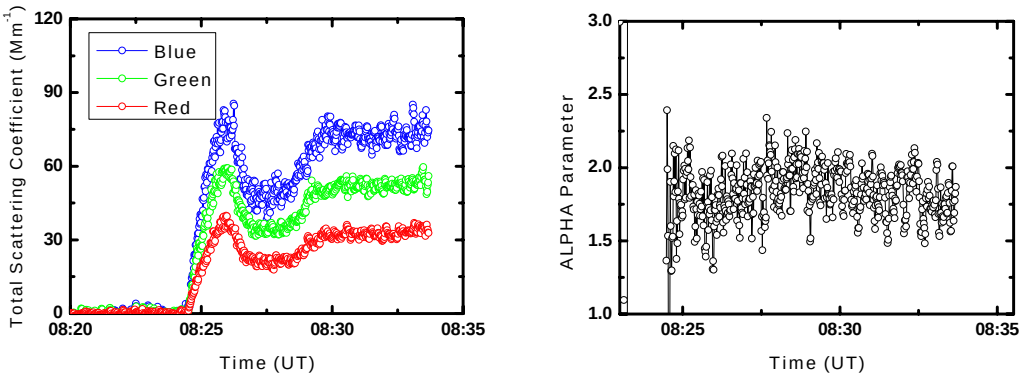

Figure 20: Total scattering coefficient and alpha parameter variation with time. The data were retrieved while the plane was taking off.

As we can see in Figure 19, there is an increment of total scattering coefficient with altitude. It means that there are more particles in high altitudes. This is strange because particle concentration should decrease with altitude in many atmospheres. However, we can say that we flew from the airport, which should be a clean area, to industrial areas over Rotterdam city. It means that we might have flown from clean to polluted area. Due to flight restrictions, we can not follow any trajectory over a city or contaminated area. Then, we can observe fluctuations with time in total scattering coefficient, with maximums and minimums. It shows that optical properties of the particles changes, which can be explained as we fly from clean to polluted areas and vice versa. The alpha parameter is around 1.8-2.1, with a maximum at about 2.1. It can be concluded that both the total scattering coefficient and alpha parameter from Figure 20 show that the particle source is urban-industrial.

·ZONE II: Flying above the sea: Track suit

After flight over Rotterdam area, we arrived to the sea and looked for ship plumes. In the next figure we can see both the total scattering coefficient and the alpha parameter evolution with altitude and time.

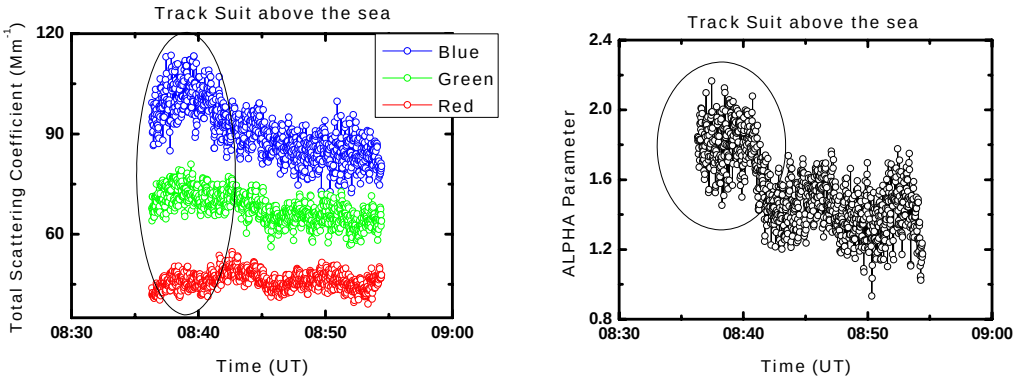

Figure 21. Time-evolution for total scattering coefficient and alpha. The data were collected while we looked for ship plumes.

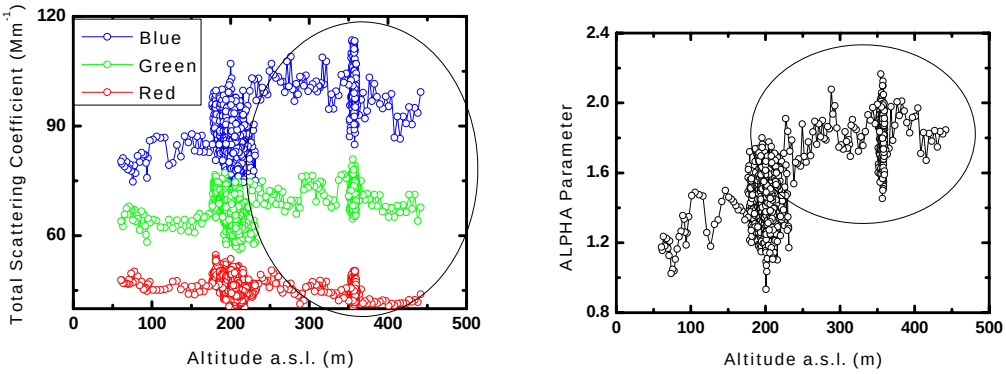

Figure 22. Total scattering coefficient and alpha parameter variation with altitude. The data were collected while we looked for ship plumes.

In the Figures 21 and 22 we can see how total scattering coefficients decrease between times 8:35 and 8:40. In these minutes, we flew from continental to maritime area. The decrease is bigger in the blue and green channel, which are more sensitive to small particles. The red channel, which is more sensitive to big particles, does not change very much. It means that we pass from an area with small particles to an area with bigger particles. The alpha time-evolution, shows also the transition from a zone over land where smaller particles predominate ($\alpha \approx 2.1\text{-}1.8$) to over sea where bigger particles predominates ($\alpha \approx 1.4\text{-}1.6$).

The results explained above can be also seen in Figure 22. When we flew over land we were at about 500-600 m and when we flew over sea we were very low (between 60-200 m more or less). At high altitudes, total scattering coefficients are bigger both in blue and red channel, while the red channel is approximately constant. The alpha parameter at high altitudes is higher ($\alpha \approx 2.1\text{-}1.8$) than low altitudes ($\alpha \approx 1.4\text{-}1.6$).

On the other hand, we found some ship plumes. We found one ship and we flew several times over its plume. In Figure 22, at about 375 m we can see that there is a strong increment in extinction coefficient in all channels. It happened while we flew over the ship plume. Furthermore, in this moment, the alpha parameter also changed quickly.

· ZONE III: Profile I:

After looking for ship plumes, we carried out an atmospheric profile from 60 m to almost 5000 m. In Figure 23 we can se the total scattering coefficient evolution with altitude.

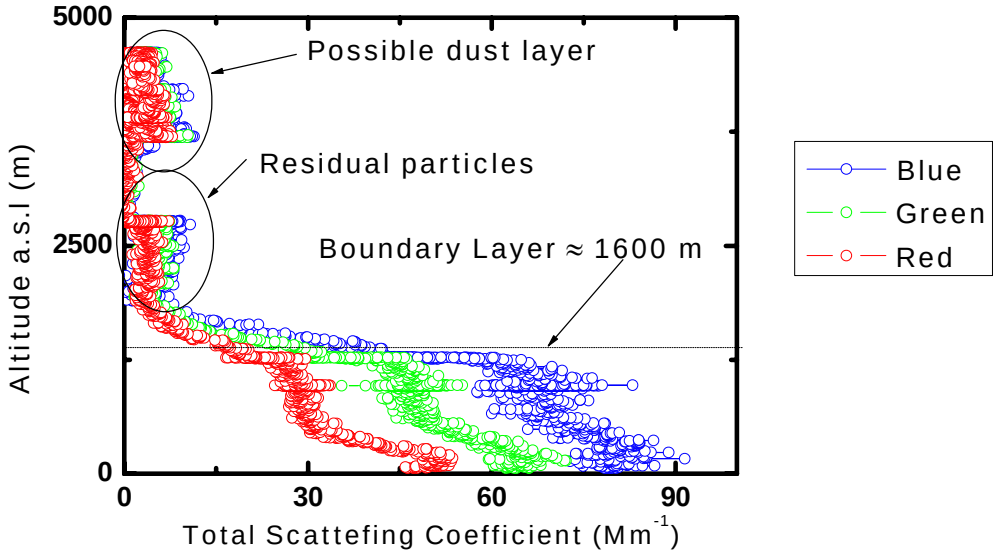

Figure 23. Total scattering coefficient evolution with altitude for our atmospheric profile over sea.

From Figure 23, we can see the total scattering coefficient decay slightly until 1600 m. Then, there is a rapid decay to zero for all channels. It happens because we have passed the top of the boundary layer, below which most particles are located. As a result, we can say that the top of the boundary layer is located at ~1600 m.

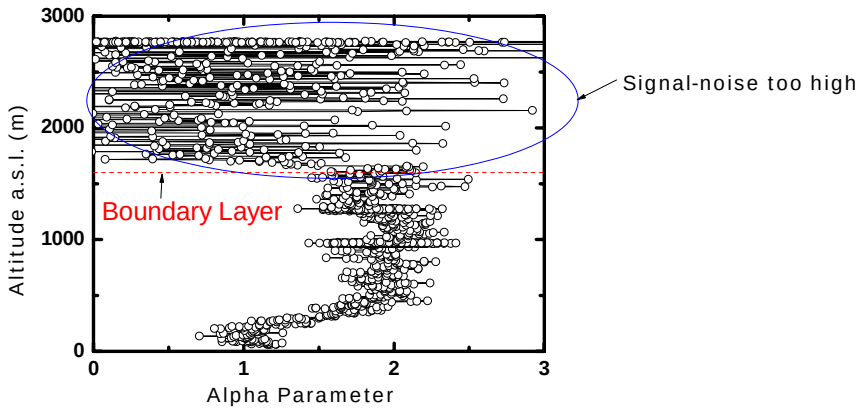

Figure 24. Alpha parameter evolution with altitude for our atmospheric profile over sea.

From Figure 24 we can see that above boundary layer the alpha parameter changes very rapidly. This happens because there are very few particles, and the scatter signal in the nephelometer is very weak. As a result, signal-noise is very high and there are small fluctuations towards zero in the total scattering coefficient that make alpha fluctuate very quickly.

On the other hand, below boundary layer we can observe how alpha parameter changes from 1 at 60 m to 2 at 500m. Later, alpha parameter is stable more or less until the boundary layer. It means that bigger particles predominate at low levels and smaller particles predominate at high levels. Maybe at low level we have sea-salt particles and

at high levels we have urban-industrial particles which might have come from the European continent. But this last must be counteracted by air mass analysis.

·ZONE IV: Possible dust layer

According to our flight briefing, we look for a possible dust layer at about 4 km. In our previous atmospheric profile, we can see that about 4500 m there is a very thin increase in the total scattering coefficient. Figure 25 shows total scattering coefficient evolution at this altitude.

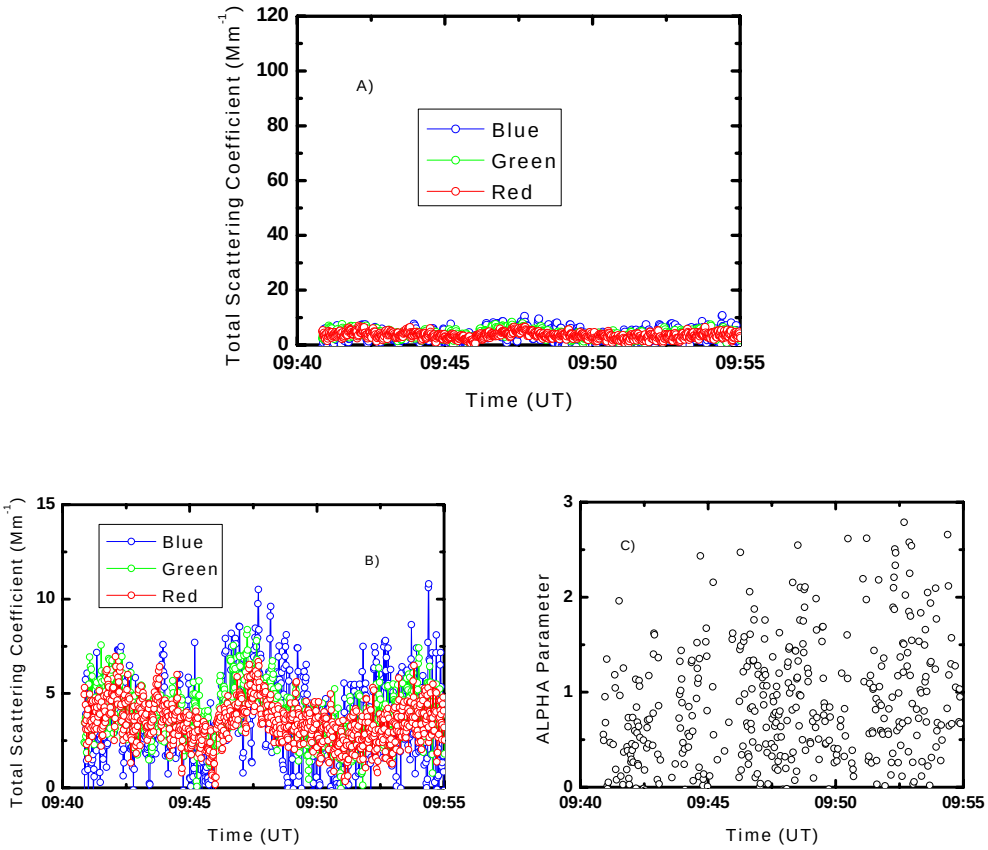

Figure 25. Total scattering coefficient evolution at 14,700 ft. At this altitude we should find a dust layer. Figure 25b is a zoom of the total scattering coefficient evolution, and Figure 25c shows the alpha parameter.

From Figure 25 we can see the total scattering coefficient is very small in all channels. However, it is distinct to zero and we can see a slight increase at about 09:48.

The alpha parameter changes really quickly because of the small fluctuations towards zero in the total scattering coefficient. Then we can say that there were too few particles in this area. As a result, we can not say that there was a dust layer at this altitude. We can say that there was only a really slight increase in the particle number.

· ZONE V: Profile II

When we reached 14,700 ft altitude, we realised that there wasn't any strong evidence of a dust layer, and so we had to make a new atmospheric profile descending to 9000 ft.

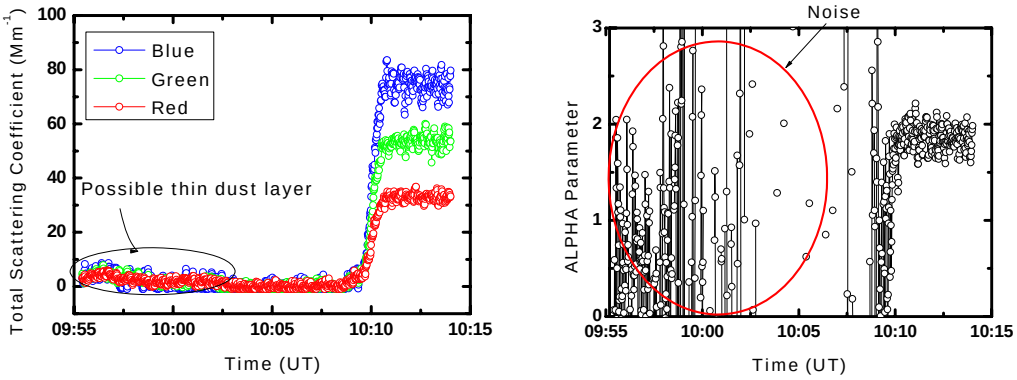

Figure 26. Time-evolution for total scattering coefficient and alpha parameter. The data were collected while we made an atmospheric profile from 14,700 ft to 9000 ft.

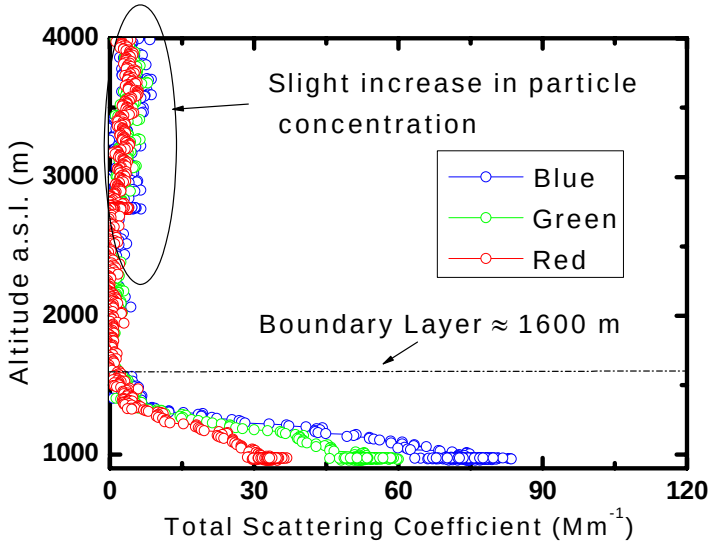

Figure 27: Total scattering coefficient for our second atmospheric profile.

In these last graphs we can see that we found our boundary layer at about 1600 m again. We observe again that there were no particles above boundary layer. We also see how below boundary layer total scattering coefficient increase as the altitude decrease. It means that the particle concentration decrease with altitude. Alpha parameter analysis shows that below boundary layer small particles predominate ($\alpha \approx 2$).

· ZONE VI: Profile III -Landing

Finally, we come back to Rotterdam airport. We were at about 1000 m and due to flight restrictions; we had to climb up to 5000 m quickly to get into the flight corridor so we could make the return transit to Rotterdam. Then, we could make another atmospheric profile from 5000 m to surface level. Figures 28 and 29 show this profile.

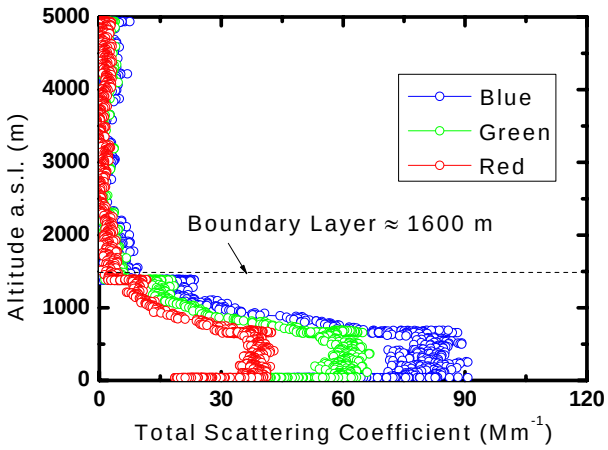

Figure 28: Total scattering coefficient for our last atmospheric profile.

From Figure 28, we observe similar results as in previous profiles. The boundary layer is located at about 1600 m. There are no particles above boundary layer. Below boundary layer, we have that the total scattering coefficient increase with altitude.

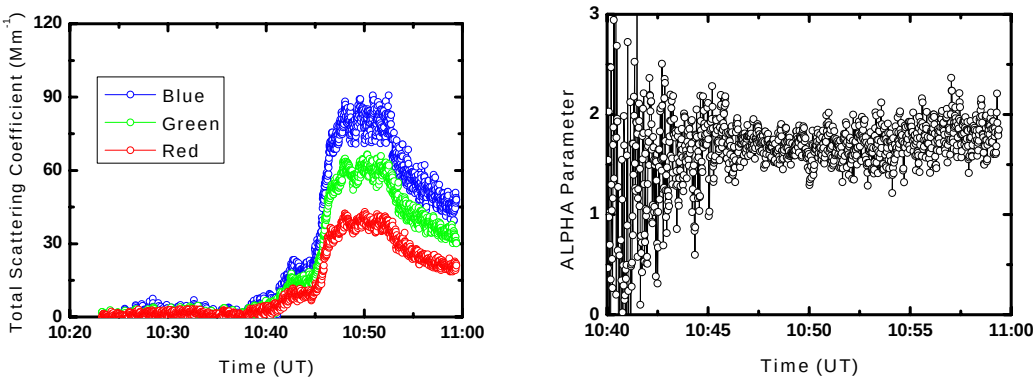

Figure 29. Time-evolution for total scattering coefficient and alpha parameter. The data were collected while we made our last atmospheric profile from 5000 m to Rotterdam airport.

In Figure 29 we can see that we reach maximum value in the total scattering coefficients for all channels, with a decrease later. As we neared the end of the flight, we flew first over an industrial area in Rotterdam city and later we took land in a cleaner area (the airport is located outside the city). The alpha parameter now is near 1.8-1.9, that is, small particles predominate. It should be because we were flying over land.

6.4 Ship plumes.

Here is a short summary of the chemical data for ship plumes. Please refer to Figure 30 below, which shows the NO_x, NO_2, NO, CO and ozone observations for this time period of the flight.

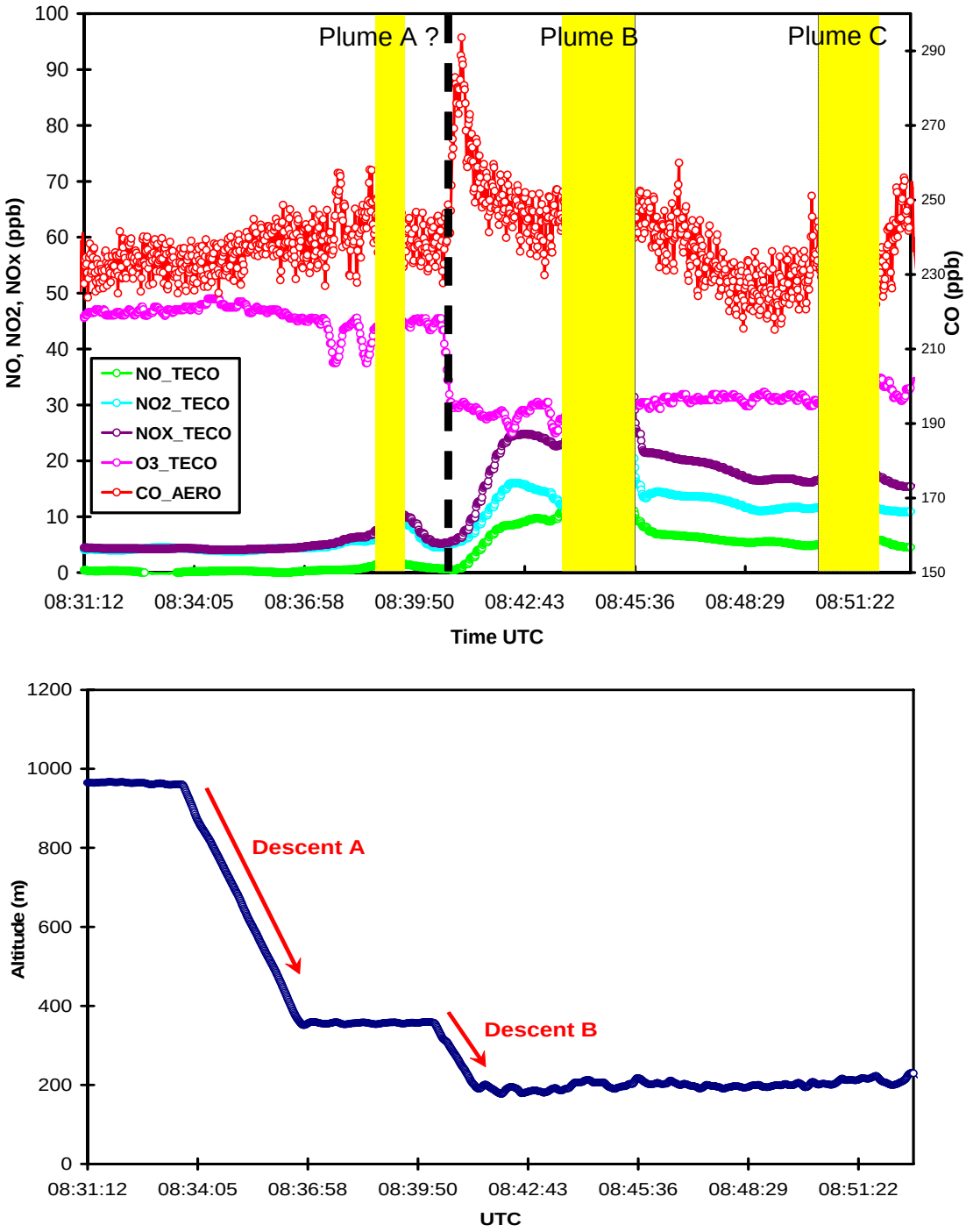

Figure 30. Chemical data for the ships plumes. Three possible plumes are identified. Plume B shows the largest spike in NO_x and the largest drop in ozone. The dashed bar indicates a sudden change in the CO and ozone measurements. There is no corresponding change in NO_x, so it is possible this is an instrument artefact associated with the change in aircraft speed.

Identifying the plumes.
According to the flight log, a ship's plume was seen at 08:38:38 UTC. There is a slight increase in NO_x at this time, though the NO_x is mostly NO_2 (recall that $NO_x = NO_2 + NO$). The smaller proportion of NO could indicate the age of the plume, since NO reacts with ozone to give NO_2. This could explain the slight drop in ozone seen, though it is unclear as to why this is seen in a different location (i.e. not coincident on the time-series).

Plume B is the most clearly defined, as we see a clear spike in the NO (24 ppb) and NO_2 (35 ppb). There is a larger NO/NO_2 ratio here, indicating proximity to the source. Because NO reacts rapidly with ozone (and with other components) it is often not seen as strongly in aged plumes. The corresponding drop in ozone is seen due tot his reaction. There is an increase in the CO as well, as this is emitted directly from combustion processes. It should also be noted that we see this at a lower altitude.

There could also be a third plume seen in the NO_2 and NO_x signals (Plume C), though the signal here is much smaller, and there is little NO seen again, indicating possibly a more aged plume.

Variation with altitude.
When comparing the chemistry plot with the altitude plot just below it in Figure 30, we can see that as we descend to lower levels, there is an overall increase in the level of NO_x and a drop in ozone. There is relatively little change in background levels of NO_x during descent A, and a larger change during descent B. There are higher levels of these pollutants closer to the sources (i.e. which are at the surface), so we can observe this gradient. The drop in ozone can be attributed to a combination of higher NO levels (which reacts with ozone), or less photochemical production of ozone.

7. CONCLUSION.

For flight B358 on 22nd April 2208, the observation area was between an area of high pressure to the north, and an area of low pressure to the south. This brought a steady easterly flow of air to the aream and the high pressure system led to fairly stable conditions with light winds. An inversion just above the boundary layer led to trapping of pollution in the boundary layer (seen in the evidence from the comparison between the two heights, Sections 6.2, and the nephelometer analysis in Section 6.3). This trapping of pollution led to a haze layer that could clearly be seen as we flew above the boudary layer.

From the comparison of the boundary layer air and the free troposphere air, it is clear that there are substantial differences between these two air masses. These differences may have been enhanced here due to the prevailing meteorological conditions. The air above the top of the boundary layer was substantially dryer than that below, as seen in the dew point data, indicating a hydro-lapse at this location.

There is a difference in the height of the boundary layer over the sea and over the land, most probably due to stronger convection above land, or by the later time of the measurements (Section 6.2.1). The difference in values over the sea could be due to instrument error, or again due to the different time of the observations, thus showing the evolution of the boundary layer.

8. ACKNOWLEDGEMENTS.

We wish to thank the wonderful crew of the BAe-146 for all their help before, during and after the flight. Also thanks to KNMI for hosting us during the course, and to EUFAR for providing this opportunity.

9. BIBLIOGRAPHY.

Baron, P.A and K. Willeke, Aerosol measurement: principles, techniques, and applications Wiley: New York, 2001.

Christensen, J. H., 1997. The Danish eulerian hemispheric model - A three-dimensional air pollution model used for the Arctic. *Atmospheric Environment,* **31**, 4169-4191.

Dubovik, O., Holben, B., Eck, T.F., Smirnov, A., Kaufman, Y.J., King, M.D., Tanré, D., Slutsker, I., 2001. Variability of absorption and optical properties of key aerosol types observed in worldwide locations. Journal of Atmospheric Sciences, **59,** 590-608.

Ferrare, R., D.D. Turner, M. Clayton, S. Guibert, M. Schulz and M. Chin, The Vertical Distribution of Aerosols Over the Atmospheric Radiation Measurement Southern Great Plains Site Measured versus Modeled. Fifteenth ARM Science Team Meeting Proceedings, Daytona Beach, Florida, March 14-18, 2005.

Ferrare, R.A., D.D. Turner, M. Chin, S. Guibert, M. Schulz, C. Chuang, M. Krol, S.E. Bauer, G. Myhre, Ø. Seland, S. Ghan, X. Liu, P. Ginoux and T. Takemura, The Vertical Distribution of Aerosols: Lidar Measurements versus Model Simulations Sixteenth ARM Science Team Meeting Proceedings, Albuquerque, New Mexico, March 27 - 31, 2006.

Guibert, S., V. Matthias, M. Schulz, J. Bösenberg, R. Eixmann, I. Mattis, G. Pappalardo, M.R. Perrone, N. Spinelli and G. Vaughan, The vertical distribution of aerosol over Europe - Synthesis of one year of EARLINET aerosol lidar measurements and aerosol transport modeling with LMDzT-INCA, *Atmos. Environ.,* 39, 2933-2943, 2005.

Gunter, L., Assessment of boundary layer variations in the Tampa Bay Area during the Bay Region Atmospheric Chemistry Experiment (BRACE). *Atmos. Environ*., 41, 4165-4176, 2007.

IPCC, Climate Change 2001, The Scientific Basis, Contribution of working Group I to the Third Assessment Report of the Intergovernmental Panel on Climate Change, Cambridge University Press, 2001.

Kovalev, V.A., Eichinger, W. E., 2004. Elastic LIDAR. Theory, practice and analysis methods. Published by John Wiley & Sons, Inc., Hoboken. New Jersey.

Matthias, V., and J. Bösenberg, Aerosol climatology for the planetary boundary layer derived from regular lidar measurements, *Atmos. Res.*, 63, 221-245, 2002.

Matthias, V., D. Balis, J. Bösenberg, R. Eixmann, M. Iarlori, L. Komguem, I. Mattis, A. Papayannis, G. Pappalardo, M.R. Perrone, X. Wang: Vertical Aerosol Distribution over Europe: statistical analysis of Raman lidar data from 10 European Aerosol Research Lidar Network (EARLINET) stations. *J. Geophys. Res.*, 109 (D18), D18201, 2004.

Nickovic, S., A. Papadopoulos, O., Kakaliagou and Kallos, G., 2001. Model for prediction of desert dust cycle in the atmosphere. *Journal of Geophysical Research*, **106**, 18113-18129.

Stohl A., Haimberger L., Scheele M. P., Wernli H. An intercomparison of results from three trajectory models. *Meteorological Applications*, 8(2):127-135, June 2001.

Weitkamp, C., 2005. LIDAR Range-Resolved optical remote sensing of the atmosphere. Edited by Claus Weitkamp, Springer.

Wernli H. and Davies H. C. A lagrangian-based analysis of extratropical cyclones. I: The method and some applications. *Quarterly Journal of the Royal Meteorological Society*, 123(538):467-489, January 1997.